Mol. Cryst. Liq. Cryst., Vol. 432, pp. 59–68, 2005

ISSN: 1542-1406 print/1563-5287 online
DOI: 10.1080/154214090892429

Taylor & Francis
Taylor & Francis Group

Fabrication of Patterned Liquid-Crystalline Nanocomposites and their Novel Characteristics

Jung-Woo Park
Weon-Sik Chae
Hee-Won Shin
Yong-Rok Kim
Department of Chemistry, Yonsei University, Seoul, Korea

Jin-Kyu Lee
School of Chemistry, Seoul National University, Seoul, Korea

Highly ordered nanostructures of liquid-crystal molecules were patterned within porous anodic alumina of different pore diameters. As the utilized pore diameter of the porous membrane decreases, progressively red-shifted emissions are observed for the embedded liquid-crystal nanostructures at room temperature. This unique spectral progression, depending on the pore size, is very similar to the emission trend induced by the thermotropic phase-transitions of the bulk antiferroelectric liquid-crystal. Such characteristics are considered to be due to structural confinement of the antiferroelectric liquid-crystal molecules within the finite size of nanoporous channels.

Keywords: antiferroelectric; confinement; liquid crystal; nanowire; porous anodic alumina

INTRODUCTION

For the past decade, porous anodic alumina (PAA) with well-ordered nanochannel arrays has often been utilized as a template to fabricate one-dimensional (1D) nanostructures of wire and tubular

This work was financially supported by National Research Laboratory (Grant No. M1-0302-00-0027), National R&D Project for Nano-Science and Technology (Grant No. M1-0214-00-0021), KRF (Grant No. BSRIDP0228), and Yonsei University Research Fund of 2002. We are grateful for the instrumental support from the equipment facility of CRM-KOSEF, Korea University.

Address correspondence to Yong-Rok Kim, Department of Chemistry, Yonsei University, Seoul 120-749, Korea. E-mail: yrkim@yonsei.ac.kr

morphologies [1]. Various functional systems of metals [2,3], semiconductors [4,5], magnets [6], and organic molecules [7–9] have been incorporated within the PAA template to obtain the high-quality 1D nanostructures after removal of the template. The pore diameter of the PAA template can be controlled by various anodization conditions of applied voltage and utilized electrolytes in electrochemical cells, and the length of the nanoporous channels can simply be tuned by anodization time [10]. Therefore, a specific 1D nanostructure can easily be fabricated by using the PAA templates of controlled dimension of the nanochannels.

Among the previously studied functional systems, organic 1D nanostructures have attracted great attention because of their facile formation within the PAA template and unique optical properties [7–9]. The organic 1D nanostructures that consist of pyrene [7] and perylene [8] are reported to show the typical red-shifted electronic transitions in optical spectra as the domain size of the system increases. Such properties are considered to be due to the weak multiple energetic couplings among the organic constituents [8].

On the other hand, in the molecular system of organic liquid crystals (LCs), strong intermolecular energetic coupling is expected and the characteristic energetic properties of thermotropic and lyotropic phases of LC molecular systems are observed in bulk and specific solution phases, respectively [11,12]. Recent studies show that the functional LC phases can be stabilized within "soft-type" templates such as crosslinked polymer matrix [13] and polymer particle network [14]. Such heterogeneous structures present the novel properties that are ascribed mainly to the interface effects: The LC molecules located at the boundary of the LC domain can be disturbed by surrounding templates.

In this study, we report on the organic nanowires consisting of antiferroelectric liquid-crystal (AFLC) molecules that are molded within the ordered PAA nanochannels of controlled pore dimension. The AFLCs have widely been studied because of the peculiar behaviors of their chiral smectic subphases. Because the electric-field-induced phase transition occurs between antiferroeletric smectic C_A^* and ferroelectric smetic C^* subphases, the AFLCs are considered to be the potential materials for field-controlled optical devices [15]. Among various AFLCs, (*R*)-4-[(1-methylheptyloxy)carbonyl]phenyl-4′-octyloxy-4-biphenylcarboxylate (R-MHPOBC, Figure 1) which has ferro- (119°C), ferri- (118°C), and antiferroelectric (66°C) phases [16–19] has widely been investigated as a prototype material for the surface-stabilized ferroelectric liquid-crystal devices [20,21]. In this report, for the new nanocomposite of the embedded R-MHPOBC within the nanoporous PAA, the interesting unique energetic and

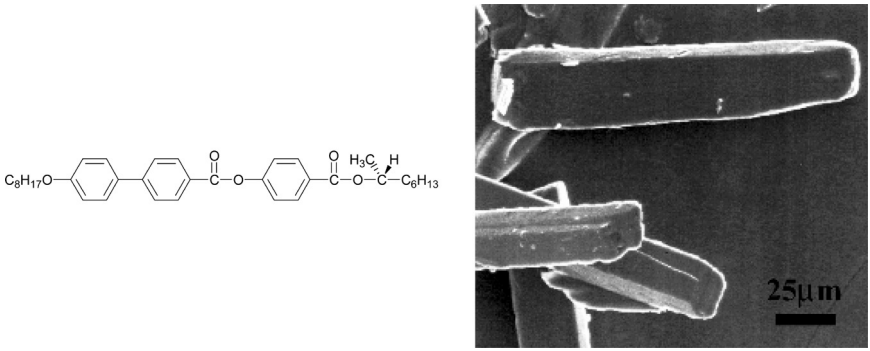

FIGURE 1 Molecular structure of the R-MHPOBC and the FE-SEM image of the bulk R-MHPOBC.

structural properties are presented and, in particular, the observed novel spectral red shift with the decreased host channel diameter is totally different from the energetic properties previously reported with the other organic nanosystems [7,8]. Such characteristics can be assumed to be due to the interface effects and the strong intermolecular couplings of LC. Furthermore, the perturbation of the molecular ordering in the interface region of the LC template may affect the molecular ordering of the vicinal LC phase. In the nanodomain of the LC surrounded by matrix, such effect can be more significant because of the enlarged portion of the LC molecules existing at the interface region. Therefore, the detailed nature of the controlled LC characteristics in various nanodomains is investigated to understand the unique energetic and structural properties of these new nanocomposites of the embedded R-MHPOBC within the nanoporous PAAs.

EXPERIMENTAL

Preparation of PAAs

To fabricate the R-MHPOBC nanostructures, the nanoporous PAAs (domain size: $1\,\text{cm} \times 1\,\text{cm} \times 10\,\mu\text{m}$) with the different pore diameters of 20, 40, and 80 nm (Figure 2) were utilized as the templates. The nanoporous PAAs were prepared by typical two-step anodizing process of aluminum plate (Aldrich, 99.999%) in controlled voltages and electrolytes as reported in the literature [7,22,23]. A constant dc voltage of 20 V was applied for the preparation of 20-nm PAA in aqueous sulfuric acid electrolyte (3 wt.%), and dc 40 V was applied to prepare the PAAs of 40 and 80 nm in aqueous oxalic acid (2 wt.%). For the preparation of

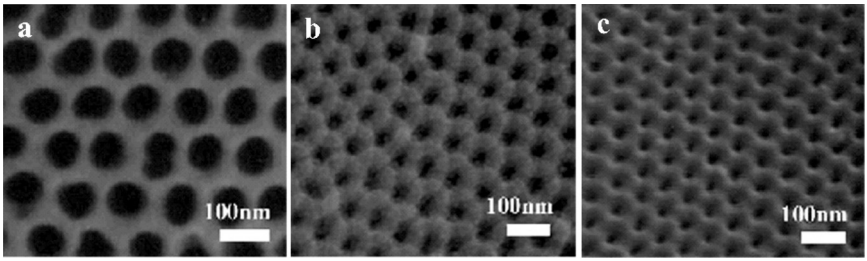

FIGURE 2 FE-SEM images of the void PAAs with the pore diameters of (a) 80, (b) 40, and (c) 20 nm.

80-nm PAA, the pore-widening process was further applied in aqueous phosphoric acid (5 wt.%) for 30 min.

Incorporation of the R-MHPOBC into the PAAs

Incorporation of the R-MHPOBC (Aldrich, 98%) into the nanoporous channels of the PAA was accomplished by the following procedure: 1) loading of the bulk LC onto the PAA membranes, 2) heating up to slightly above the melting point (156°C), and 3) infilteration of the molten viscous LC molecules into the nanoporous PAAs by partial capillary force within the PAA nanochannels during the heating and evacuating conditions ($\sim 10^{-2}$ Torr). To study the embedded morphology of R-MHPOBC, the PAA template was removed in 1M NaOH aqueous solution at room temperature (RT) and subsequently washed several times with distilled water to eliminate excess NaOH residual.

Characterizations

A field emission scanning electron microscope (FE-SEM, Hitachi S-4200) with the acceleration voltage of 5–10 kV was applied to study the morphologies of the fabricated R-MHPOBC nanocomposites, bulk R-MHPOBC, and R-MHPOBC nanowires as well as the PAA template membranes of different pore diameters. Emission spectra were obtained with a fluorescence spectrophotometer (Hitachi F-4500). A X-ray diffractometer (Mac Science M03XHF[22]) was applied to analyze the structural characteristics.

RESULTS AND DISCUSSION

Figure 3 shows the FE-SEM images of the nanostructures of R-MHPOBC incorporated into the PAAs with different pore diameters.

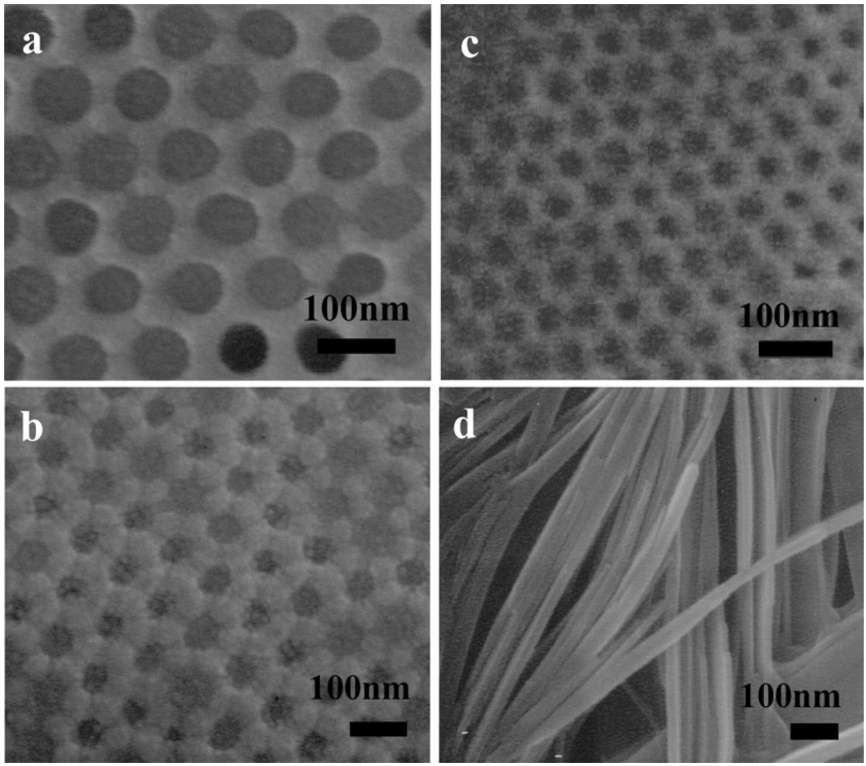

FIGURE 3 FE-SEM images of the patterned R-MHPOBC nanostructures within the PAAs with pore diameters of (a) 80, (b) 40, and (c) 20 nm; (d) R-MHPOBC nanowires after removal of the 40-nm PAA.

The R-MHPOBC molecules are well embedded within the hexagonal nanopores of the PAAs with different pore diameters, although a few void nanoporous channels still remained (Figure 3a–c). The nanostructural morphology of the R-MHPOBC formed within the PAA is further confirmed after removal of the PAA template, showing the membrane-free R-MHPOBC nanowires (Figure 3d). The R-MHPOBC nanowire has a diameter of approximately 40 nm, which is very similar with the nanochannel size of the utilized PAA template, whereas the bulk R-MHPOBC crystal shows long plate shape with the width and the length of $\sim$25 μm and $\sim$150 μm, respectively (Figure 1).

Figure 4 is the emission spectra of the R-MHPOBC embedded within the PAAs of different pore diameters along with that of the solid-state bulk. Interestingly, the emission spectra show the size-dependent spectral red shift for the R-MHPOBC incorporated

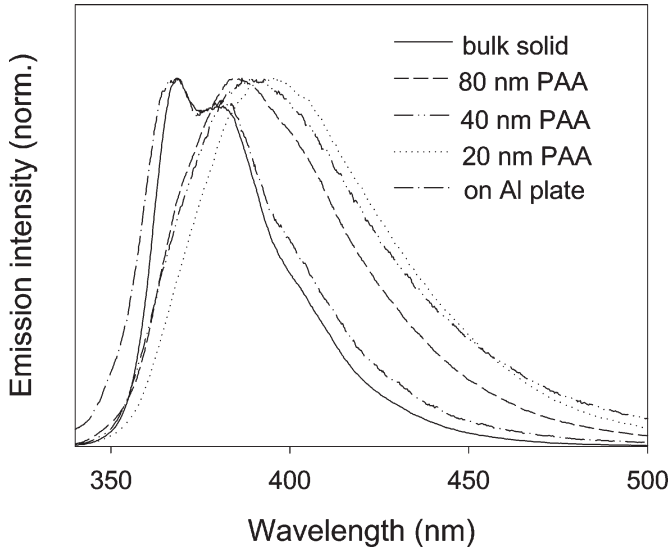

FIGURE 4 Emission spectra of the R-MHPOBC at RT: bulk (solid line), coated form on aluminum plate (dash-dotted line), and embedded forms within the PAAs with pore diameters of 80 (short-dashed line), 40 (dash-double dotted line), and 20 nm (dotted line).

within the PAA as the pore diameter of the utilized PAA decreases. The emission spectra of the R-MHPOBC nanostructures are broadened and positioned at longer wavelengths (peaked at 385–400 nm) than the emission spectrum (peaked at ~370 nm) for the bulk R-MHPOBC. To confirm that the observed spectral shift did not come from other bulk LC phases possibly stabilized during the heating or cooling process, the emission spectrum was checked for R-MHPOBC, which was simply coated on a plain aluminum plate without nanopores and also treated by the same heating and cooling processes with the applied procedure for the formation of the R-MHPOBC nanostructures. The observed spectrum from the simple surface-coated and heat-treated R-MHPOBC exhibited no significant difference compared with that of the corresponding bulk, except for the slight spectral broadening. Therefore, it is very likely that the observed novel pore-size-dependent emission characteristics come from the confinement effect of the R-MHPOBC within the PAA nanochannels. Furthermore, it is noteworthy that this red-shifted spectral progression with the reduced nanodimension is contrary to those in the previously reported nanostructures of small organic molecules [7,8].

The size-dependent spectral progression of the R-MHPOBC nanostructures embedded within the PAAs shows, interestingly, a trend very similar to the thermotropic emission spectral shift of the bulk R-MHPOBC in terms of the spectral red shift and broadening (Figure 5). In particular, two emission spectra of the bulk R-MHPOBC measured at 85 and 130°C have spectral positions and shapes similar to the spectra for the nanostructured R-MHPOBC with 80-, 40-, and 20-nm diameters at RT. Such similarity in the spectral position and shape possibly implies that the molecular ordering and the energetic couplings in the R-MHPOBC nanocomposites with different degrees of confinement at RT resemble those in the thermotropic LC phases of the bulk R-MHPOBC.

The spectral shift and broadening in relation to the pore size of the PAA template nanochannel can be a result of the interface effects. According to the previous reports, it is known that the interface affects the morphology of the boundary between the confined polymers or small organic molecules and the corresponding PAA nanochannels [7,24]. In particular, it was recently reported that the molecular alignment of organic LC molecules located on the surface of substrates is completely different from that of the corresponding bulk and shows distinctly different phase-transition temperature for the surface LC

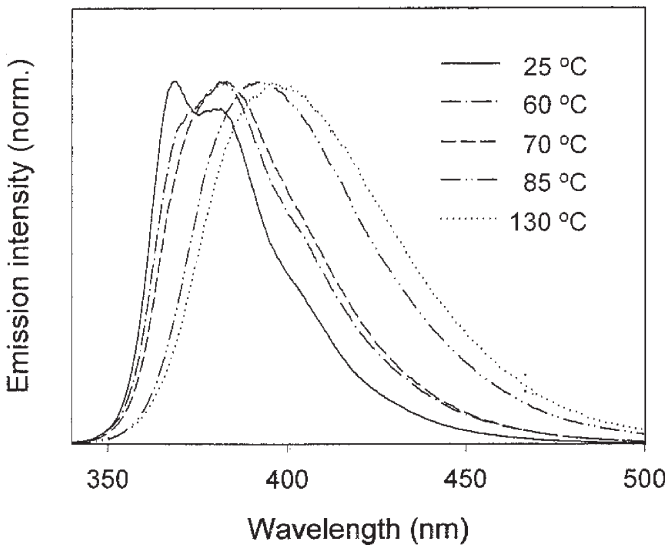

FIGURE 5 Emission spectra of the bulk R-MHPOBC at various temperatures: 25 (solid line), 60 (dash-dotted line), 70 (short dashed line), 85 (dash-double dotted line), and 130°C (dotted line).

phases, whose transition temperatures can be tuned by changing substrates [25]. In nanoconfined system, such interface-induced effects can be expected to be enhanced because of the large inner surface (or interface) to volume ratio. The large coupling effect at the host–guest interface region in nanodomain suggests that the observed unique phenomena in these nanocomposites of the embedded R-MHPOBC within the PAA are possibly a result of the modified molecular alignment at the LC-PAA interface region. Because the LC has strong intermolecular coupling forces as compared with other organic molecular systems, the coupled and modified outermost R-MHPOBC molecules of the nanowire near the surrounding wall of the PAA nanochannel may induce the inner molecular alignment of the R-MHPOBCs within the nanowire through a series of molecular

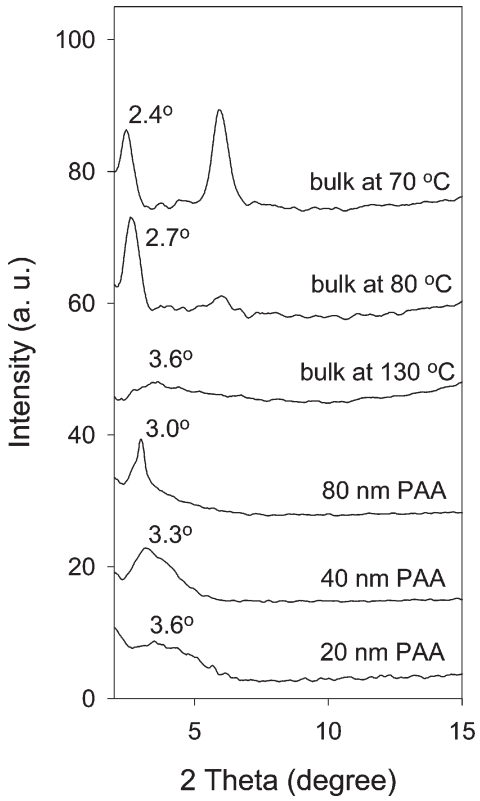

FIGURE 6 X-ray diffractions of the bulk R-MHPOBC at different temperatures and the confined R-MHPOBC within the PAAs of various pore diameters at RT.

couplings, resulting in the totally modified molecular alignment within the nanowire.

The X-ray diffraction analysis for the R-MHPOBC nanocomposites shows the induced molecular alignment of the R-MHPOBC within the PAA nanochannel (Figure 6). It is very interesting that the diffraction peaks (3.0–3.6° in 2θ) of the R-MHPOBC embedded within the PAA nanochannels at RT are located within the range of the diffraction peaks (2.7 and 3.6° in 2θ for the diffraction of the smectic-like layer structure [17]), which represent the thermotropic phases of the bulk R-MHPOBC at 80 and 130°C. As the utilized nanochannel decreases in diameter, the nanocomposites show the gradual diffractional peak shift from 3.0 to 3.6°, which is the same as the peak (3.6°) of the bulk R-MHPOBC at 130°C. Therefore, the confined R-MHPOBC within the 20-nm channels of the PAA template at RT must have a very similar structural property to the bulk R-MHPOBC at 130°C. The X-ray diffraction study, which implies the structural correlation between the size-dependent structure of the R-MHPOBC nanocomposites and the thermotropic subphases of the bulk R-MHPOBC, is in good agreement with the interpretation from the emission study.

Therefore, it is suggested that the observed novel feature of the phase change of the R-MHPOBC nanocomposites are triggered by the interface coupling forces, which depend on the pore diameter of the PAA nanochannels, which are completely different from the conventional thermotropic or lyotropic LC phase transitions with respect to the driving forces for the transitions.

CONCLUSIONS

The patterned LC nanostructures of the aligned nanowire morphologies were obtained by fabricating the R-MHPOBC molecules into the nanoporous PAA templates. The unique phase changes as a result of pore size are observed for the R-MHPOBC-PAA nanocomposites and show good correlation to the thermotropic phase transition of the bulk R-MHPOBC. In particular, the similarity of the phase of the R-MHPOBC in the 20-nm PAA channels at RT and the phase of the bulk R-MHPOBC at 130°C suggests a possible new methodology for LC phase transition.

REFERENCES

[1] Hulteen, J. C. & Martin, C. R. (1997). *J. Mater. Chem.*, *7*, 1075.
[2] Martin, B. R., Dermody, D. J., Reiss, B. D., Fang, M., Lyon, L. A., Natan, M. J., & Mallouk, T. E. (1999). *Adv. Mater.*, *11*, 1021.

[3] Sehayek, T., Vaskevich, A., & Rubinstein, I. (2003). *J. Am. Chem. Soc.*, *125*, 4718.
[4] Routkevitch, D., Bigioni, T., Moskovits, M., & Xu, J. M. (1996). *J. Phys. Chem.*, *100*, 14037.
[5] Xu, D., Shi, X., Guo, G., Gui, L., & Tang, Y. (2000). *J. Phys. Chem. B*, *104*, 5061.
[6] Nielsch, K., Wehrspohn, R. B., Barthel, J., Kirschner, J., Gösele, U., Fischer, S. F., & Kronmüller, H. (2001). *Appl. Phys. Lett.*, *79*, 1360.
[7] Lee, J.-K., Koh, W.-K., Chae, W.-S., & Kim, Y.-R. (2002). *Chem. Commun.*, 138.
[8] Zhao, L., Yang, W., Ma, Y., Yao, J., Li, Y., & Liu, H. (2003). *Chem. Commun.*, 2442.
[9] Zhao, L., Yang, W., Zhang, G., Zhai, T., & Yao, J. (2003). *Chem. Phys. Lett.*, *379*, 479.
[10] Li, A. P., Müller, F., Birner, A., Nielsch, K., & Gösele, U. (1998). *J. Appl. Phys.*, *84*, 6023.
[11] Lee, M., Kim, J.-W., Hwang, I.-W., Kim, Y.-R., Oh, N.-K., & Zin, W.-C. (2001). *Adv. Mater.*, *13*, 1363.
[12] Hwang, I.-W., Choi, H.-H., Cho, B.-K., Lee, M., & Kim, Y.-R. (2000). *Chem. Phys. Lett.*, *325*, 219.
[13] Kikuchi, H., Yokota, M., Hisakado, Y., Yang, H., & Kajiyama, T. (2002). *Nature Mater.*, *1*, 64.
[14] Meeker, S. P., Poon, W. C. K., Crain, J., & Terentjev, E. M. (2000). *Phys. Rev. E*, *61*, R6083.
[15] Chandani, A. D. L., Ouchi, Y., Takwzoe, H., Fukuda, A., Terashima, K., Furukawa, K., & Kishi, A. (1989). *Jpn. J. Appl. Phys.*, *28*, L1261.
[16] Fukui, M., Orhihara, H., Yamada, Y., Yamamoto, N., & Ishibashi, Y. (1989). *Jpn. J. Appl. Phys.*, *28*, L849.
[17] Hori, K. & Endo, K. (1993). *Bull. Chem. Soc. Jpn.*, *66*, 46.
[18] Toriumi, H., Yoshida, M., Mikami, M., Takeuchi, M., & Mochizuki, A. (1996). *J. Phys. Chem.*, *100*, 15207.
[19] Hou, I., Schacht, J., Gieelmann, F., & Zugenmaier, P. (1997). *Liq. Cryst.*, *22*, 401.
[20] Clark, N. A. & Lagerwall, S. T. (1980). *Appl. Phys. Lett.*, *36*, 899.
[21] Mederious, D. R., Hale, M. A., Leitko, J. K., & Willson, C. G. (1998). *Chem. Mater.*, *10*, 1805.
[22] Masuda, H. & Satoh, M. (1996). *Jpn. J. Appl. Phys.*, *35*, L126.
[23] Li, F., Zhang, L., & Metzger, R. M. (1998). *Chem. Mater.*, *10*, 2470.
[24] Steinhart, M., Wendorff, J. H., Greiner, A., Wehrspohn, R. B., Nielsch, K., Schilling, J., Choi, J., & Gösele, U. (2002). *Science*, *296*, 1997.
[25] Boamfa, M. I., Kim, M. W., Maan, J. C., & Rasing, Th. (2003). *Nature*, *421*, 149.